doi:10.1093/mnras/stz1073





Velocity and orbital characteristics of micrometeors observed by the Arecibo 430 MHz incoherent scatter radar

Yanlin Li and Qihou Zhou*

Department of Electrical and Computer Engineering, Miami University, Oxford OH45056, US

Accepted 2019 April 1. Received 2019 March 30; in original form 2018 July 5

ABSTRACT

Using the Arecibo 430 MHz incoherent scatter radar located in Puerto Rico, we report the characteristics of the smallest meteors observed by any ground-based instruments. Coupled with an efficient pulse coding technique, the radar detects over 40 meteors \min^{-1} in the dawn hours. The typical mass of these meteors is estimated to be 10^{-13} kg and the corresponding radius is about 2 μ m. The velocity of the meteors is concentrated within a narrow range at a given time from mid-night to noon. Numerical simulations show that such a characteristic is most consistent with meteoroids having circular orbits in inclined planes. The orbital evolution of these meteoroids is most significantly affected by Poynting–Robertson and solar wind drags. They are captured by the Earth on their way to spiral into the Sun. At the mass range where drag forces dominate, Earth-crossing meteoroids are mostly expected to be in quasi-circular orbits because they can be produced anywhere outside the Earth's orbit. Our observation demonstrates this is indeed the case for retrograde meteoroids.

Key words: interplanetary medium – meteorites, meteors, meteoroids – zodiacal dust.

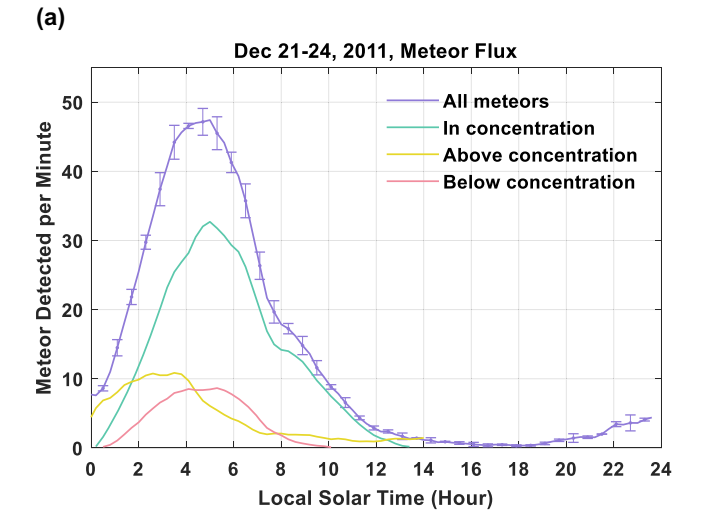
1 INTRODUCTION

Incoherent scatter radars (ISRs) are high power and large aperture radars used to measure incoherent scattering from the ionosphere. ISRs typically operate at very-high-frequency (VHF) and ultrahigh-frequency (UHF) range from 50 MHz to 1.3 GH. Although they have been used for ionospheric studies since the 1960s, their consistent use for meteor detection did not start until the 1990s (Chapin & Kudeki 1994: Pelline-Wannberg & Wannberg 1994; Zhou, Tepley & Suzler 1995). Traditional low-power meteor radars typically operate around 50 MHz and detect meteor trails perpendicular to the radar boresight. UHF radars operating around 400 MHz are not sensitive to meteor trails because of their rapid expansion beyond the radar wavelength. Instead, UHF radars mainly detect scattering from the high-density plasma in the meteor head region, i.e. the head echo. In the last two decades, all major highpower large aperture radars in the world have been used for meteor observations (e.g. Zhou, Mathews & Nakamura 2001; Close et al. 2002: Janches et al. 2003: Chau, Woodman & Galindo 2007: Kero et al. 2012; Schult et al. 2018). This report is mainly concerned with ISR head-echoes observed at Arecibo, Puerto Rico (18.3°N, 66.8°W).

The Arecibo ISR consists of a 300 m in diameter dish, a 1.5 MW transmitter, and a cryogenic receiver with the sky and system temperature combining to 90 K, making it the most sensitive radar in

the world. Using time-integrated data, the initial study by Zhou et al. (1995) established the fact that the Arecibo ISR detects the faintest meteors of any ground observation. By counting the flux rate, they estimate the equivalent visual magnitude as +14. Subsequent pulseresolved observations reveal that these echoes typically last less than 40 ms in the radar beam (Zhou & Kelley 1997). The pulse-resolved observations make it possible to determine meteor velocity and deceleration (Janches et al. 2000; Mathews et al. 2001). Mathews et al. (2001) estimate the mass range of the Arecibo meteors to be 10^{-14} – 10^{-7} kg and the radius in the range of 1–200 μ m, with the upper bound being observed only at a rate of 1 per day. In comparison, Kero et al. (2008) estimate the mass range observed by the EISCAT UHF radar to be 10^{-9} – $10^{-5.5}$ kg. Sulzer (2004) indicates that the majority of the early morning meteors are in circular orbits coming from the apex direction.

The data we use for this report were taken from 2009 June 19–21 and 2011 December 21–24. In both observations, we used the coded-long-pulse technique as in Sulzer's (2004) study. The transmitted pulse consists of 220 binary-coded bits with each bit having a duration of 2 μ s. The inter-pulse-period (IPP), i.e. the time duration between two adjacent transmitted pulses, is 10 ms. Complex samples are taken at 2 μ s time intervals, yielding a range resolution of 300 m. The data processing procedure for meteor detection is largely the same as described in Sulzer (2004). The long pulse used in our observations allows the detection of the faintest meteors of any ground-based observations and the most accurate measurement of velocities. We analyse the salient characteristics of the meteors observed by the Arecibo radar and discuss their implications on the evolution of meteoroid orbits.



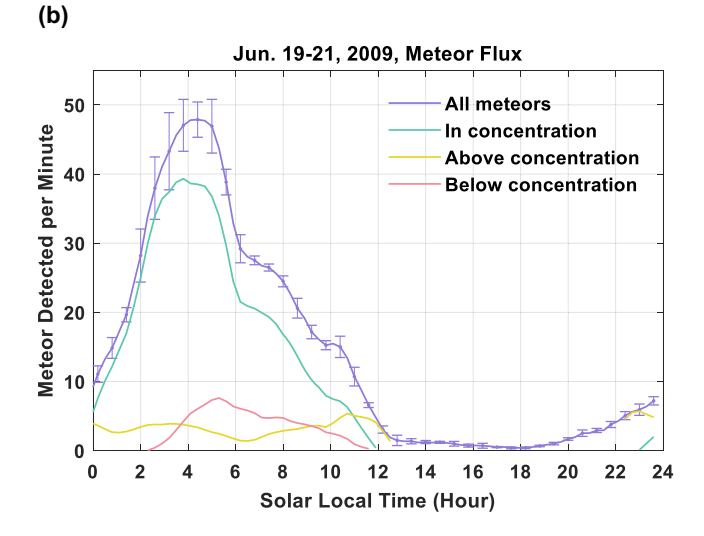


Figure 1. Averaged meteor flux rate observed by the Arecibo radar during 2011 December 21–24 (a) and 2009 June 19–21 (b). The error bars represent day-to-day variation during each period. Purple line is for all meteors detected.

2 METEOR FLUX AND DAILY VARIABILITY

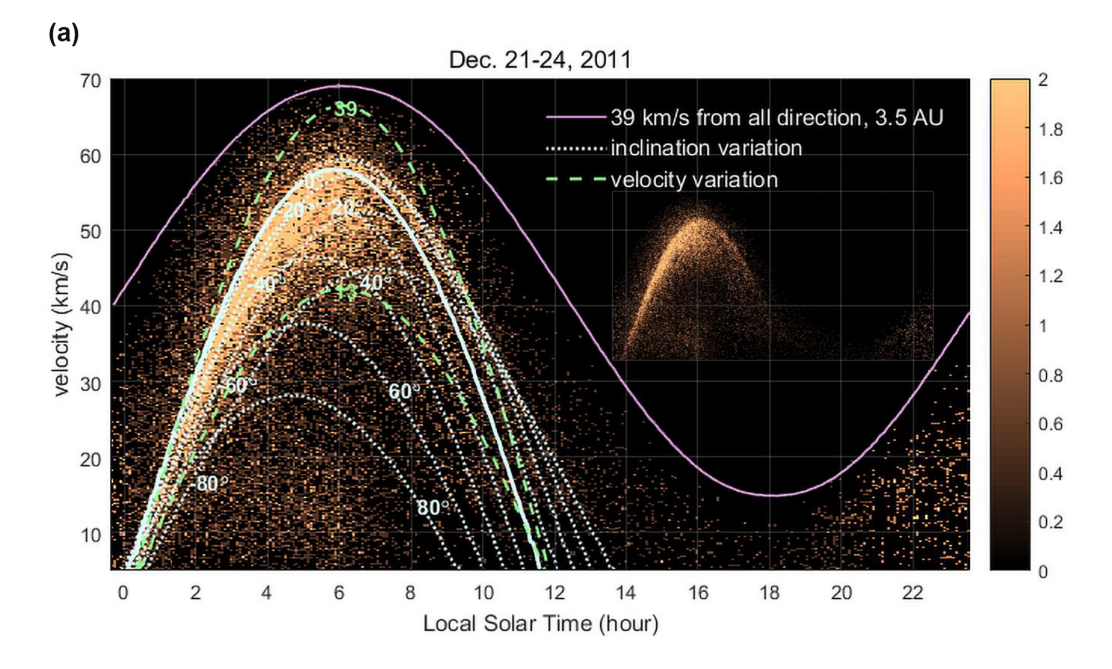
Fig. 1 shows the meteor flux rate for 2011 December 21–24 (a) and 2009 June 19–21 (b), and the root-mean-square day-to-day variation within each period. The flux rate is normalized to the operational time of the code-long-pulse (CLP). In the same figure, we also show the flux rates of three subgroups to be discussed later. The maximum flux rate, occurring at dawn, detected by the CLP technique is the highest reported at Arecibo despite the fact that the 10 ms IPP used in our observation will miss more than half of the meteors that last less than 5 ms. The flux rate at dusk, however, is not significantly improved from previous observations at Arecibo (e.g. Zhou & Kelley 1997; Mathews et al. 2001; Janches et al. 2003).

One key difference between the observations used for this report and previous studies is the radar pulsing frequency, or inversely, the IPP. Our present study uses a 10 ms IPP while the IPP in previous studies ranged from 1 and 2 ms at Arecibo. Although the 1–2 ms IPP configuration can catch more short-lived meteors, the noise floor is increased due to range aliasing. For example, in the case of 1 ms IPP, meteor echo from 100 km is mixed with ionosphere returns from

250, 400, 550 km, etc. The bulk of the ionosphere above Arecibo lies between 100 and 600 km and is highly dynamic, especially during the nighttime. The noise level of 1 ms IPP can be more than 30 times of that of 4 ms IPP (Zhou 2000) in the D-region below 90 km during nighttime. Although the difference at 100 km is not as dramatic as at 90 km, it is fairly common for the noise level of 1 ms IPP to be several times higher than that of the 10 ms IPP for meteor detection. Because the E-region ionosphere is much stronger during the day than night, this gives rise to the asymmetry of meteor rates with respect to the local sunrise time around 6:00 am. Since meteor detection threshold is based on signal to noise ratio (S/N), change in noise level (i.e. ionosphere) directly affects the detection rate. Observations using a 10 ms IPP do not suffer from the range aliasing effect although they are still subject to the noise power variation at meteor heights. Overall, day-to-day variability using a 10 ms IPP is far less sensitive to ionosphere variability than the 1-2 ms IPPs. The small day-to-day flux rate variability, shown as error bars in Figs 1(a) and (b), indicates that the micrometeor population at 1 au is very stable. The observed variability for the mass range sensitive to the Arecibo ISR is within that of the background ionosphere and radar pointing direction relative to the ecliptic plane. This is in clear contrast to the strong daily variability observed in-situ by the Long Duration Exposure Facility (McDonnell et al. 2001). Other studies indicate strong seasonal variations (e.g. Mathews et al. 2001; Campbell-Brown & Jones 2006). Although our data do not appear to indicate any seasonal variation, this aspect has to be ascertained by the analysis of more data.

3 METEOR SIZE AND MASS

Using the meteoroid momentum equation and observed deceleration, Mathews et al. (2001) estimate that the meteors observed by the Arecibo ISR operating in the 1 ms IPP mode is in the mass range of 10^{-14} – 10^{-7} kg. Another way to estimate the mass is through the flux rate. The Arecibo radar beam size at 100 km is largely the size of the dish with a radius of 150 m. The 10 ms pulse spacing in our observations means that there is only a 50 percent chance to catch a meteor when it lasts 5 ms. On the other hand, meteors do not come down straight into the beam. Oblique meteors tend to increase the effective receiving area of the radar. These two factors compensate each other. Using an effective detection area of π 150 ² m², a rate of 40 meteors min⁻¹ is equivalent to a cumulative flux of 10^{-5} meteors s⁻¹ m⁻², or 1.5×10^{17} meteors yr⁻¹ over the entire surface of the Earth. Such a cumulative flux rate puts the typical mass in our observation at 10^{-13} kg using the table found in Grun et al. (1985) or Ceplecha (1998). The meteor rate in Mathews et al.'s (2001) study is about an order of magnitude lower than our present observation. One order of magnitude difference in flux rate translates to 2.5 order of magnitude difference in mass according the mass-flux table in Grun et al. (1985). Using Mathews et al.'s (2001) result as the baseline and the Grun et al.'s (1985) mass-flux slope, the meteors in our observation would have a mass of 10^{-15} kg instead of 10^{-13} kg. For a typical mass density of $2.5-3 \times 10^3$ kg $\rm m^{-3}, \, a \, mass \, of \, 10^{-15} \, \, \, kg$ corresponds to a radius of 0.4 $\mu \rm m.$ One potential explanation for the difference between the deceleration and flux methods is that the former computes a meteoroid's mass during ablation while the latter estimates the initial mass before ablation. Another possibility is that mass and radar detectability are not strongly related. Although our current observations detect weaker echoes, it is possible that the majority of them come from the same mass range as from Mathews et al.'s observation but with less ionization efficiency.



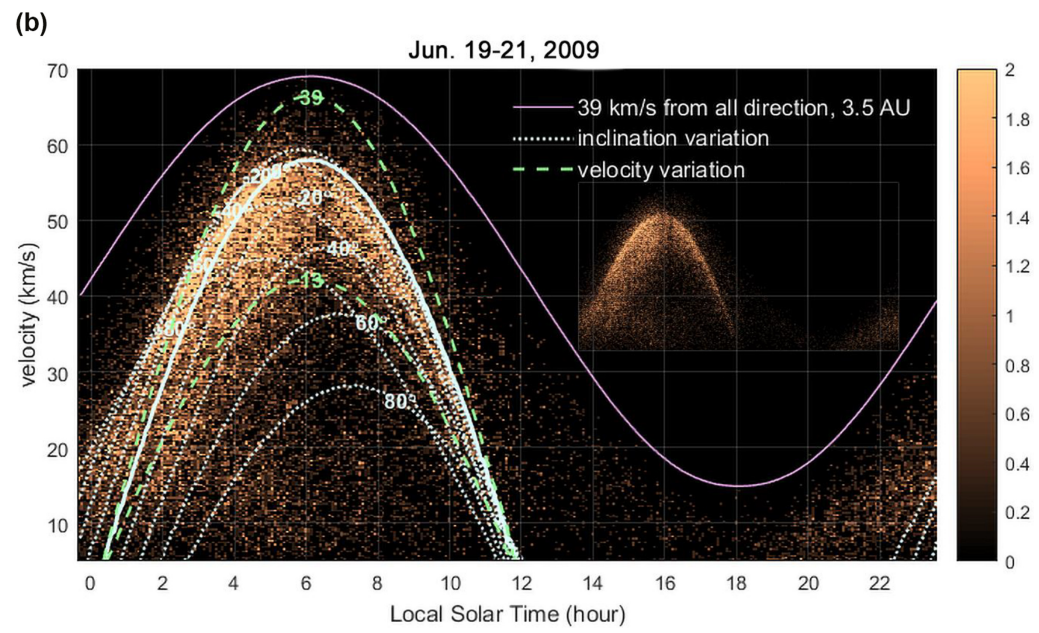


Figure 2. Meteor velocity distribution as a function of time for 2011 December 21–24 (a) and 2009 June 19–21 (b). The colour code indicates the number of meteors observed per minute and per $\mathrm{km}\,\mathrm{s}^{-1}$. Solid blue curve is the expected radar velocity for meteors on circular orbit in the ecliptic plane. The two dashed green curves are the expected radar velocities for meteors in the ecliptic plane having a heliocentric velocity of 13 and 39 $\mathrm{km}\,\mathrm{s}^{-1}$, respectively. The dotted blue curves are for meteors on circular orbit with varying inclination. The pink line is the limiting radar velocity for meteors having a heliocentric velocity of 39 $\mathrm{km}\,\mathrm{s}^{-1}$ and semimajor axis of 3.5 au. The insert contains only the velocity distribution highlighting the region of higher concentration.

While our current study does not contribute directly to the methods of mass calculation, determination of orbits puts a strong constraint on the range of meteor mass. Particles with a radius smaller than 1 μ m is subject to severe radiation pressure and will likely evolve into hyperbolic orbits before being blown out of the solar system (Dermott et al. 2001). As discussed below, the meteoroids in our observations are mostly in quasi-circular orbits – implying that their radius should be larger than 1 μ m. The more realistic mass and radius in our observation, therefore, are likely 10 $^{-13}$ kg and 2 μ m, respectively. Such a mass and size put the Arecibo observations in the range of spacecraft observations (Fechtig, Leinert & Berg 2001).

4 VELOCITY DISTRIBUTION

The Doppler velocity of a meteor in the radar line-of-sight direction can be accurately determined. Monte Carlo simulations for a typical S/N show the accuracy is about 0.1 km s⁻¹. As the Arecibo radar was pointed vertically throughout our observations, all the observed velocities were in the zenith direction. The zenith velocity of all meteors observed as a function of time is shown in Figs 2(a) and (b) for 2011 December and 2009 June, respectively. The colour code indicates the number density per km s⁻¹ and per minute. The observed meteors are clearly seen to concentrate in an arc region

from mid-night to noon when the radar was on the forward side of the Earth as it revolves around the Sun. The insert in Fig. 2 is the same as the full-scale figure without the obstruction of the superimposed lines. The velocities around the dawn hours are predominantly in the range of 45–60 km, indicating that the majority of the meteors observed are in retrograde orbits. Away from the dawn hours when the angle between the radar boresight and the tangent of the Earth's orbit increases, the line-of-sight velocity largely reduces as a 'sinusoidal' variation. Another salient feature of the velocity distribution is that the velocity spread between mid-night to dawn is much narrower than that between dawn and noon in December while the opposite is true in June.

To understand the orbital characteristics of the meteors observed by the Arecibo radar, we model the observed velocities for meteors on various orbits. In our model, we place many meteoroids with an assumed initial vector velocity evenly in a 'spawning semisphere', which is a semisphere 20 times of the Earth's radius (R_e) on the front side of the Earth. The subsequent orbits of the meteoroids are simulated using the Euler method by considering the gravity interactions of the Sun and the Earth. The Moon's gravity is not considered as it has an insignificant effect on a meteoroid's trajectory when it is relatively close to the Earth. The radius of the 'spawning semisphere' is chosen to minimize the initial error caused by Earth's gravity potential, which accelerates a particle of $30 \text{ km s}^{-1} \text{ by } 0.1 \text{ km s}^{-1} \text{ when it reaches the spawning semisphere,}$ and to have a reasonable computational efficiency at the same time. If a meteoroid reaches an altitude of 100 km above the Earth's surface, the impact location, radial, and vector velocities are recorded along with its initial conditions. For each inclination angle and initial velocity, we do not terminate the simulation until 100 000 meteoroids have reached the surface of the Earth. The simulation allows us to obtain an expected radar velocity at any location of the Earth for each assumed meteoroid orbit. For example, the solid blue line in Figs 2(a) and (b) is obtained by selecting the zenith velocities of all meteoroids landing at 18.3°N with the spawning meteoroids in the ecliptic plane and having a velocity of 30 km s⁻¹. This line largely follows the concentration arc in both figures.

To explain the velocity spread, we consider two alternative hypotheses: (1) meteoroids in the ecliptic plane have different heliocentric velocities; (2) meteoroids are in circular orbits but have different inclinations. The dashed green curves in Fig. 2 show the expected radar velocities when spawning meteoroids are in the ecliptic plane with a heliocentric velocity of 13 and 39 km s⁻¹, respectively. The two velocities are chosen to cover most of the meteors in the concentration region. While we see that the majority of the meteors in the concentrated region falls between these two curves, they cannot account for the asymmetry between the predawn and post-dawn hours for the same period as well as the difference between the December and June periods.

In Fig. 2, the dashed blue lines show the expected radar velocities from meteoroids in circular orbits but at different inclination angles. For the winter period, we see that meteoroids originating from drastically different inclinations have a much narrower spread in the predawn hours than the post-dawn hours, in agreement with the observation. The narrow concentration at mid-night is because the radar pointing direction aligns very closely with the Sun-Earth connection line (which forms a 5° angle with the radar boresight at mid-night). In such a geometry, all meteors in circular orbits have their trajectories nearly perpendicular to the radar boresight, yielding a very small line-of-sight velocity, irrespective of the inclination angle. At winter solstice noontime, the radar boresight has an angle of 41° with the Sun-Earth connection line, allowing a

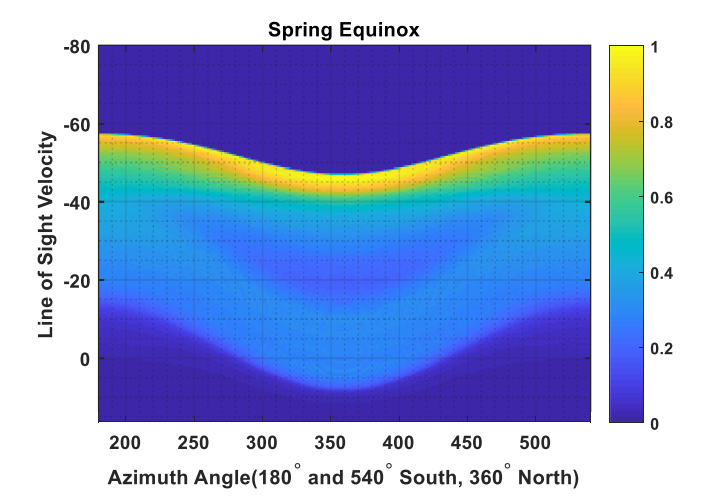
large range of line-of-sight velocities to be observed from different inclination angles. The largest velocity occurs when the inclination is 90° . This velocity is $20.2~{\rm km\,s^{-1}}$ with the Earth's gravitational field considered. As seen from Fig. 2(a), the circular orbit model matches with the winter observation very well.

A critical test for the circular but different inclination model is to examine the distribution at other seasons. Because the tilt of the Earth's rotational axis with respect to the Sun varies with season, the narrow band between mid-night and dawn, and the wide band between dawn and noon in the winter solstice observed in Fig. 2(a) are expected to be reversed in the summer solstice. This is indeed what the observation shows, as seen in Fig. 2(b).

Sulzer (2004) presented the results from autumn and spring equinoxes with the radar continuously moving at a zenith angle of 15°. The observed distributions of meteors as the azimuth angle are shown as figs 7 and 12 for the autumn and spring equinox respectively in Sulzer (2004). As a meteor's vector velocity from any inclination at any location can be found from the orbital simulation described above, using the flux rate shown in Fig. 1 and the inclination distribution discussed below, we plot the simulated azimuth angle distribution for autumn and spring equinoxes in Fig. 3. Further details on all the simulations presented in this report are discussed in Li (2019). The simulated results without assuming any source distribution or atmospheric deceleration capture the most important features in Sulzer's observations – the upper edge variation for both seasons and the concentrated region at the highvelocity end. Although Sulzer (2004) was also able to model the azimuth distributions, he had to use different parameters for different seasons to match the observations.

While most of the meteors fit into the inclined circular model, some of meteors are clearly in ecliptic orbits. The meteors in the concentration band within the declination range of -80° to 80° is about 71 per cent of all the meteors observed on the forward side of the Earth. As a meteoroid having a velocity higher than 30 km s $^{-1}$ on an eccentric orbit can fall into the concentration band as well, the relative number of meteors in circular orbit is somewhat lower than 71 per cent. The green curve in Fig. 1 shows the flux rate as a function of time for meteors inside the concentration, which we interpret to be largely the rate of meteors on circular orbits.

The distribution as a function of inclination angle can be found through solving an inversion problem by counting all the meteors in each inclination and time grid. Equivalently, we can also assume an initial distribution and adjust it to minimize the error between the observation and the model through iterations. We use the latter method as it is easier to implement. In deriving the inclination distribution, we divide all the inclinations from -90° to 90° into 180 1° cells and initialize all the cells with an equal number of test meteors, say, 100. For a given inclination distribution and a local time, a velocity distribution can be calculated for circular orbits. For each time interval of 20 min, we find the differences between the velocity distribution of the test meteors with the observations shown in Fig. 2 and output the sum of the absolute differences. Next, we adjust the inclination distribution by randomly moving a test meteor from one cell to another to create a slightly different inclination distribution, whose velocity distribution is again calculated and compared with the observation. If the new sum of the absolute differences is smaller than the previous one, the change is accepted and the distribution is updated. Otherwise, the change is rejected and the previous distribution is kept. Iterate the process until the sum of the absolute differences is minimized to produce an inclination distribution for each time interval. Fig. 4 is the average of the distributions from approximately mid-night to noontime. Further



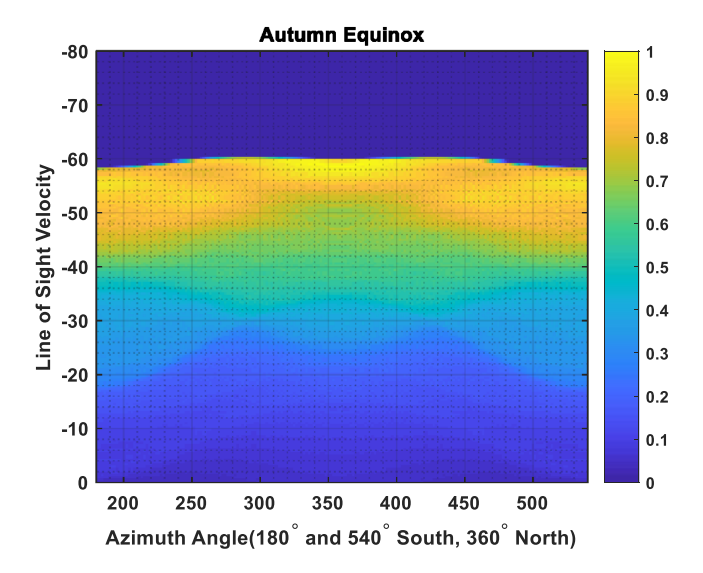


Figure 3. Simulated meteor density distribution as a function of azimuth angle for spring (upper panel) and autumn (lower panel) equinoxes. The simulations can explain the observed characteristics reported in Sulzer (2004).

details on the process as well as a performance analysis can be found in Li (2019). In both periods, we see that the majority of the meteors have an inclination angle centred around $+50^{\circ}$ (ascending from south) and -30° (descending from north). Previous orbit study of Arecibo meteors by Janches, Meisel & Mathews (2001) assumed that meteor trajectory is in the beam pointing direction. Their orbital parameters are likely not reliable as the majority of the meteors are detected at a considerable angle with the radar boresight.

Using the Jicamarca ISR located in Peru, Chau et al. (2007) reported sporadic sources in the direction of northern/southern apex (centred at $\pm 13^{\circ}$), hellion/antihelion, and north/south toroidal directions (centred at $\pm 55^{\circ}$) that are typically observed by meteor radars. Similar radiant distributions in the Sun-centred ecliptic coordinates are also reported by the Middle and Upper (MU) atmosphere radar and Middle Atmosphere ALOMAR Radar System (MAARSY), which are somewhat less sensitive than the Jicamarca radar (Kero et al. 2012; Schult et al. 2018). Our observations from Arecibo, unfortunately, cannot be plotted in the Sun-centred ecliptic

longitude because of the lack of vector velocity observations. With our assumption of circular orbits, Fig. 4 is effectively a vertical cut at the Sun-centred ecliptic longitude of 270° (i.e. the plane perpendicular to the ecliptic containing apex). While the inclination distribution shown in Fig. 4 may strongly depend on instrument selection effect, the Arecibo radiant distribution appears to be quite different from those observed by the Jicamarca or other VHF meteor radar systems. This difference is understandable because the Arecibo meteoroid population is more in line with those observed by spacecraft, as discussed in Section 3, than with the VHF observations. Despite that the Jicamarca radar has about the same aperture and transmitter power as the Arecibo ISR, higher operating frequency at Arecibo makes it orders of magnitude more sensitive than the Jicamarca ISR especially considering that scattering from head-echoes is in the Rayleigh regime.

When discussing the orbital characteristics of meteoroids, it is important to consider atmospheric drag on meteors from which we derive the velocities. Although most of the meteors are observed only in one or two pulses, some of them last over 10 pulses allowing us to see the deceleration clearly over an altitude range of several kilometres. The reduction in velocity from the highest altitude of observation to 105 km is less than 1 km s⁻¹, which is also supported by calculations based on momentum equation for a meteoroid mass of 10^{-13} kg. Reduction in velocity from 105 to 99 km is about 3 km s⁻¹ for a meteor descending at 60 km s⁻¹ but negligible for a meteor descending at 20 km s⁻¹. Atmospheric drag has minimum effect on half of the meteors observed above 105 km. It is possible that atmospheric drag may have a significant effect for meteors observed below 95 km but their number is relatively small (5.5 per cent). (All of the meteors in our observations are above 90 km due to the long radar pulse used.) As seen in Fig. 2, the lowvelocity region is more likely associated with positive than negative inclination angles, it is possible that the higher rate observed near 30° than at -50° in Fig. 4 may be due to atmospheric drag. This, however, is a secondary effect. The most important aspects on orbital discussion, i.e. the narrow concentration bands before and after dawn, respectively for winter and summer solstices, and their consistency with the assumption of circular orbits, are not affected by atmospheric drag effect.

5 METEORS IN NON-CIRCULAR ORBITS

We have focused on meteors within the concentration band, which we interpret to be largely on circular orbit with different inclinations. Meteors above the concentration band in Fig. 2 have a heliocentric velocity larger than 30 km s⁻¹ at the interception with the Earth's orbit. The relative number of such meteors is 15 percent out of all the forward side meteors. Unlike the main group within the concentration band, the flux rate of this group, shown as a yellow line in Fig. 1, does not exhibit the characteristic diurnal variation. In Figs 2(a) and (b), we also include the expected maximum observable velocity for meteors having a heliocentric velocity of 39 km s⁻¹ (equivalent to a semimajor axis of 3.5 au). Out of the 63 000 meteors observed, only three of them are above this line and none of them has a demonstrable hyperbolic velocity. As the majority of the meteors within the concentration band are in circular orbits due to drag forces, meteors above the concentration band are also expected to be affected by the same forces. Their orbits have not evolved into nearly circular ones yet.

Meteors below the concentration band have low line-of-sight velocities. Their relative proportion is 14 percent and their flux rate as a function of time is plotted as a red line. They consist of

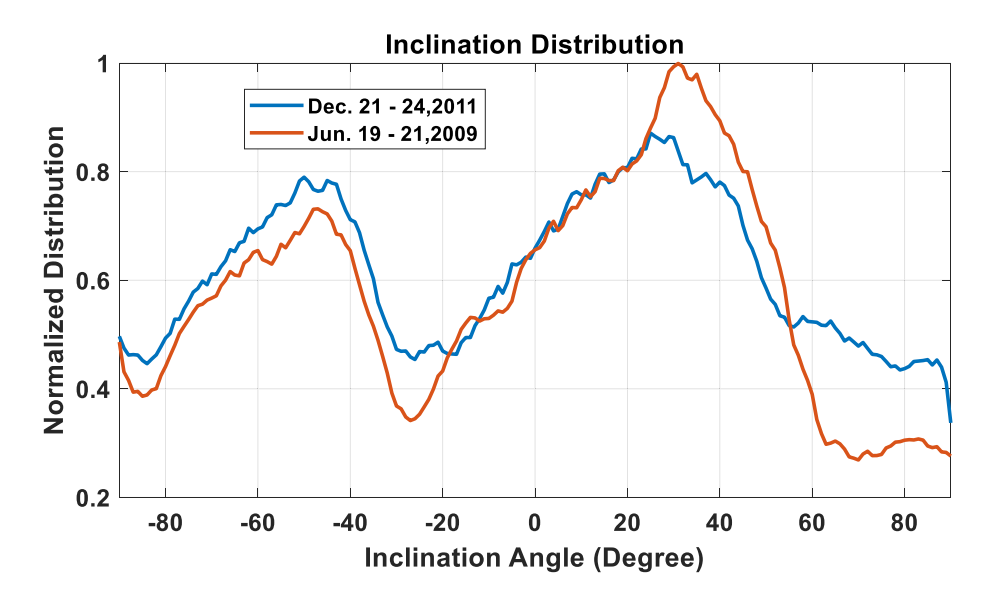


Figure 4. Normalized meteor distribution as a function of inclination angle for 2011 December 21–24 and 2009 June 19–21 for all meteors observed from mid-night to noon. Descending from south is defined as positive.

prograde meteors on low-eccentricity orbits caught up by the Earth and meteors with high eccentricity either in retrograde or prograde orbits. The atmospheric velocity for the meteors above, inside and below the concentration band decreases in that order. Although we only observe in the vertical direction, meteor ablation height generally correlates very well with the vector velocity of a meteor. The average ablation height for the three groups of meteors is 105, 103, and 99 km, respectively. Meteors observed on the back-side of the Earth are largely prograde meteors with a heliocentric velocity larger than 30 km s $^{-1}$. Their detection rate is very low because of small atmospheric entry velocity.

6 DISCUSSION AND CONCLUSION

The most important aspect of the current report is the conclusion that the majority of the meteors observed by the Arecibo radar are in nearly circular orbits. This points to the importance of Poynting-Robertson and solar wind drags. The nature of the two drags is similar, with the latter being about 30 per cent of the former (Gustafson 1994). In order for the drag forces to be effective, meteoroid mass is typically smaller than 10^{-11} kg. On the other hand, when β , the ratio of radiation pressure to solar gravitation force, is larger than 0.5, a particle will be blown out of the solar system. $\beta = 0.5$ corresponds to a particle size of 1 μ m (Dermott et al. 2001) and a mass of 10^{-14} kg, which is the lower boundary of the meteors observed at Arecibo as discussed above. Thus, Arecibo meteors appear to have the 'Goldilocks' size, small enough for the drags to force them into nearly circular orbits and being pulled inward to the Sun but large enough not to be blown away by the radiation pressure. The simulations by Borin et al (2017) show that it takes several million years to reduce the semimajor axis from 3.4 to 1 au for a 10 μ m in radius particle. The evolution time for the smaller Arecibo particles is expected to be much shorter.

As the Earth lies relatively close to the Sun, the majority of the meteoroids have their initial orbits outside that of the Earth whether they are of asteroidal or cometary origin. For meteoroids whose size is right for drag forces to be important, their orbits will evolve

into nearly circular ones at 1 au if not rejected by gravitational scattering by outer planets. Meteoroids with a diameter of 1-9 μ m originating from as far as the Kuiper belt have a 20 per cent chance of reaching 1 au and once a meteoroid's orbit reaches within that of Jupiter, it will largely spiral onto the Sun (Liou, Zook & Dermott 1996). As all meteoroids in the mass range of 10^{-14} 10^{-11} kg generated outside Earth's orbit have a good chance to be on nearly circular orbits when they reach the inner solar system, their population is thus expected to be uncharacteristically large at 1 au. Further, meteoroids in the ecliptic plane have a higher probability ejected by outer planets than those on inclined planes. Although the distribution shown in Fig. 4 is a convolution of instrument aspect sensitivity and the true distribution, it indicates at least that a large number of meteoroids exist in inclined orbits. The 'inclined' population discussed by Divine (1993) has low eccentricity and a mean mass of 10^{-11} kg. This population largely matches our observation. However, such a population is considered to be no more than 15 per cent of the total flux model synthesized from space missions (Grun et al. 1985; Staubach, Grun & Matney 2001). Thus, our observation appears to be the first to demonstrate the theoretical expectation that meteoroids sensitive to drag forces are mostly on quasi-circular orbits at 1 au. The meteoroid characteristics in our observations may have important implications on our understanding on the production and orbital evolution of micro-meteoroids.

In conclusion, the meteors reported here are the smallest observable by any ground-based instrument. About two thirds of these meteors are on retrograde circular orbits with significant inclinations. The mass range is just right for the drag forces to play a significant role to pull the meteoroids into nearly circular orbits at 1 au on their way to the Sun.

ACKNOWLEDGEMENTS

The Arecibo Observatory is a facility of the National Science Foundation operated under cooperative agreement by University of Central Florida. The study is partially supported by NSF grant AGS-1744033. The raw data used for the analysis can be obtained from the Arecibo Observatory.

REFERENCES

- Borin P., Cremonese G., Marzari F., Lucchetti A., 2017, A&A, 605, A94 Campbell-Brown M. D., Jones J., 2006, MNRAS, 367, 709
- Ceplecha Z., Borovicka J., Graham E. W., Revelle D. O., Hawkes R. L., Porubcan V., Simek M., 1998, Space Sci. Rev., 84, 327
- Chapin E., Kudeki E., 1994, J. Geophys. Res., 100, 23811
- Chau J. L., Woodman R. F., Galindo F., 2007, I carus, 188, 162
- Close S., Oppenheim M., Hunt S., Dyrud L., 2002, J. Geophys, Res., 107, 1295
- Dermott S. F., Thomas J. J., Grogan K., Durda D. D., Jayaraman S., Kortenkamp S. J., Wyatt M. C., 2001, Interplanetary Dust. Springer, Berlin
- Divine N., 1993, J. Geophys. Res., 98, 17029
- Fechtig H., Leinert C., Berg E. O., 2001, Interplanetary Dust. Springer, Berlin
- Grun E., Zook H. A., Techtig H., Giese R. H., 1985, Icarus, 66, 244
- Gustafson B. A. S., 1994, Annu. Rev. Earth Planet. Sci., 22, 553
- Janches D., Matehws J. D., Meisel D. D., Zhou Q. H., 2000, Icarus, 145, 53
- Janches D., Meisel D. D., Mathews J. D., 2001, Icarus, 150, 206
- Janches D., Nolan M. C., Meisel D. D., Mathews J. D., Zhou Q. H., Moser D. E., 2003, J. Geophys. Res., 108, 1222

- Kero J., Szasz C., Pellinen-Wannberg A., Wannberg G., Westman A., Meisel D. D., 2008, Ann. Geophys., 26, 2217
- Kero J. et al., 2012, MNRAS, 426, 135
- Li Y., 2019, MS thesis, Miami Univ
- Liou J. C., Zook H. A., Dermott S. F., 1996, Icarus, 124, 429
- Mathews J. D., Janches D., Meisel D. D., Zhou Q. H., 2001, Geophys. Res. Lett., 28, 1929
- McDonnell T., McBridge N., Green S. F., Ratcliff P. R., Gardner D. J., Griffiths A. D., 2001, Interplanetary Dust. Springer, Berlin
- Pellinen-Wannberg A., Wannberg G., 1994, J. Geophys. Res., 99, 11379
- Schult C., Brown P., Pokorný P., Stober G., Chau J. L., 2018, I carus, 309, 177
- Staubach P., Grun E., Matney M., 2001, Interplanetary. Springer, Berlin Sulzer M., 2004, Atmos. Chem. Phys., 4, 947
- Zhou Q. H., 2000, Geophys. Res. Lett., 27, 1803
- Zhou Q. H., Kelley M. C., 1997, J. Atmos. Solar-Terr. Phys., 59, 739
- Zhou Q. H., Tepley C., Suzler M., 1995, J. Atmos. Terr. Phys., 57, 421
- Zhou Q. H., Mathews J. D., Nakamura T., 2001, Geophys. Res. Lett., 38, 1399

This paper has been typeset from a T_EX/I_AT_EX file prepared by the author.